Available online at www.sciencedirect.com
SCIENCE DIRECT
Journal of Hydrology 315 (2005) 126–153
Journal of Hydrology
www.elsevier.com/locate/jhydrol

Spatially distributed energy balance snowmelt modelling in a mountainous river basin: estimation of meteorological inputs and verification of model results

David C. Garen[a,*], Danny Marks[b]

[a]United States Department of Agriculture, Natural Resources Conservation Service, National Water and Climate Center, 1201 NE Lloyd Boulevard, Suite 802, Portland, OR 97232, USA
[b]United States Department of Agriculture, Agricultural Research Service, Northwest Watershed Research Center, 800 Park Boulevard, Plaza IV, Suite 105, Boise, ID 83712-7716, USA

Received 5 January 2004; revised 18 February 2005; accepted 18 March 2005

Abstract

A spatially distributed energy balance snowmelt model has been applied to a 2150 km^2 drainage basin in the Boise River, ID, USA, to simulate the accumulation and melt of the snowpack for the years 1998–2000. The simulation was run at a 3 h time step and a spatial resolution of 250 m. Spatial field time series of meteorological input data were obtained using various spatial interpolation and simulation methods. The variables include precipitation, air temperature, dew point temperature, wind speed, and solar and thermal radiation. The goal was to use readily available data and relatively straightforward, yet physically meaningful, methods to develop the spatial fields. With these meteorological fields as input, the simulated fields of snow water equivalent, snow depth, and snow covered area reproduce observations very well. The simulated snowmelt fields are also used as input to a spatially distributed hydrologic model to estimate streamflow. This gives an additional verification of the snowmelt modelling results as well as provides a linkage of the two models to generate hydrographs for water management information. This project is a demonstration of spatially distributed energy balance snowmelt modelling in a large mountainous catchment using data from existing meteorological networks. This capability then suggests the potential for developing new spatial hydrologic informational products and the possibility of improving the accuracy of the prediction of hydrologic processes for water and natural resources management.
Published by Elsevier B.V.

Keywords: Spatial interpolation; Meteorological variables; Snowmelt; Energy balance; Spatially distributed hydrologic modelling

1. Introduction

Spatially distributed hydrologic modelling is becoming more and more commonplace. Such models have advantages in improving both the spatial resolution of the simulation and the conceptualization

* Corresponding author. Tel.: +1 503 414 3021; fax: +1 503 414 3101.
E-mail address: david.garen@usda.gov (D.C. Garen).

0022-1694/$ - see front matter Published by Elsevier B.V.
doi:10.1016/j.jhydrol.2005.03.026

of physical processes by the model. In mountainous areas where snow is a significant part of the hydrologic cycle, snowmelt is a primary water input to the soil and stream system. It is, therefore, essential to simulate snow accumulation and melt accurately. Spatially distributed hydrologic modelling in mountainous areas first requires spatially distributed snowmelt modelling.

Various models have been developed and applied for simulating snowmelt and resulting streamflow, ranging from simple degree-day approaches (e.g. Rango and Martinec, 1995; United States Department of Agriculture—Agricultural Research Service, 1998) to full energy balance models (e.g. Blöschl et al., 1991a,b; Tarboton et al., 1995; Marks et al., 1999b). Although degree-day and other temperature-based snowmelt models (such as Anderson, 1973) can often be successful, they only work when conditions are 'typical', based on historical data, so that there is a consistent and definable relationship between temperature and snowcover energy exchange. They cannot accurately simulate complex situations, such as rain on snow, or other conditions where temperature is not likely to be a good surrogate for the energy input to the snowpack. In addition, they often require intervention by the model user to make parameter adjustments, which are sometimes subjective or not well defined. These adjustments are made throughout the snowmelt season in response to events or changing conditions to compensate for situations and processes that the model does not adequately describe. (In fact, it is just these considerations that led Kustas et al. (1994) to add energy balance components to the degree-day-based Snowmelt Runoff Model (United States Department of Agriculture—Agricultural Research Service, 1998) to improve simulation results.) Due to data and computing limitations, most past applications of energy balance snowmelt models have been restricted to small research catchments. With continuing rapid advances in meteorological data collection, geographic information systems, and computing power, constraints to using energy balance models over large areas are becoming increasingly less restrictive. It is, therefore, worthwhile to explore the application of a more physically based energy balance model, which explicitly handles relevant processes and avoids the limitations of simpler, less robust models, in mountainous river basins.

Initial applications of an energy balance snowmelt model to large mountainous areas are described by Garen and Marks (1996) and Marks et al. (1999b), while Susong et al. (1999) presented an initial discussion of methods and issues associated with developing spatial field time series of meteorological data required as input to this model over large areas. The research described in this paper is a continuation of these efforts to refine the modelling procedures and to work toward making the model usable in an operational mode. There are several objectives:

(1) develop and implement procedures for estimating spatial field time series of the necessary meteorological input data required for spatially distributed modelling
(2) demonstrate the use of the additional meteorological data not collected at most stations that are needed to support snowcover energy balance modelling (relative humidity, wind speed, solar and thermal radiation)
(3) demonstrate the application of a spatially distributed energy balance snowmelt model in a large mountainous river basin, using multiple methods to verify the model results
(4) couple the snowmelt model to a spatially distributed hydrologic model to simulate streamflow and other hydrologic variables

The snowmelt model used is called *isnobal* (Marks et al., 1999b), which is part of the UNIX-based Image Processing Workbench software package (Marks et al., 1999a). Previous applications of *isnobal* and its point version, *snobal*, are described by Marks et al. (2001), Marks et al. (1999b), and Marks et al. (1998). The test basin used in the current research represents the largest area in which the *isnobal* model has been applied.

Objectives 1 and 2 are discussed first, while objectives 3 and 4 are addressed in the sections on modelling results. The ultimate goal of this research is to demonstrate the use, practicality, and potential of spatially distributed hydrologic models for snowcover and streamflow forecasting and for water and natural resources management.

2. Description of area, data, and model runs

The test area for this study is a 2150 km^2 portion of the Boise River basin in the state of ID, USA (Fig. 1). This is the drainage area above the stream gauging station on the Boise River near Twin Springs, which is most of the inflow to Arrowrock Reservoir. It is in a mountainous region, with an elevation range of 1000–3200 m. Most of the area is coniferous forest (55%) or shrubland (20%), with the rest being either rock, grass, deciduous forest, or burned/harvested forest. Average annual precipitation ranges from about 500 mm in the lower elevations to over 1500 mm in the highest mountains, most of which occurs as snow. The basin is a major part of a large system of reservoirs and canals providing water for irrigated agriculture and for the urban Boise area. To illustrate the operational potential of this modelling approach, we have focused on this basin because it is important from a water resources management standpoint but is not a research basin, that is, the meteorological stations are ones within standard operational networks. There are some typical limitations in the data network, such as not as good of an elevational range in the data sites as might be wished, a possible bias in siting toward forest clearings, and not as fine of a time resolution as might be desired for very detailed modelling; the Boise basin, however, is fairly well instrumented for areas in the western US.

There are eight meteorological stations in and near the basin (Table 1, Fig. 1) that are available to provide input data. Three of these stations, operated by the US Bureau of Reclamation (the first three in Table 1), have precipitation and temperature data at a 15 min resolution, and one of these (Atlanta Town) also has snow water equivalent. Five stations (the last five in Table 1), part of the Natural Resources Conservation Service (NRCS) SNOTEL network, have precipitation, temperature, and snow water equivalent at a 3 h resolution. Three of these five also have solar radiation, wind speed, relative humidity, snow depth, and soil moisture and temperature sensors, which were installed in the fall of 1996 to demonstrate the collection of these additional data at standard SNOTEL sites and to support this modelling project. Also available to assist with the estimation of dew point temperature and wind speed in the higher elevations are twice-per-day upper air soundings at

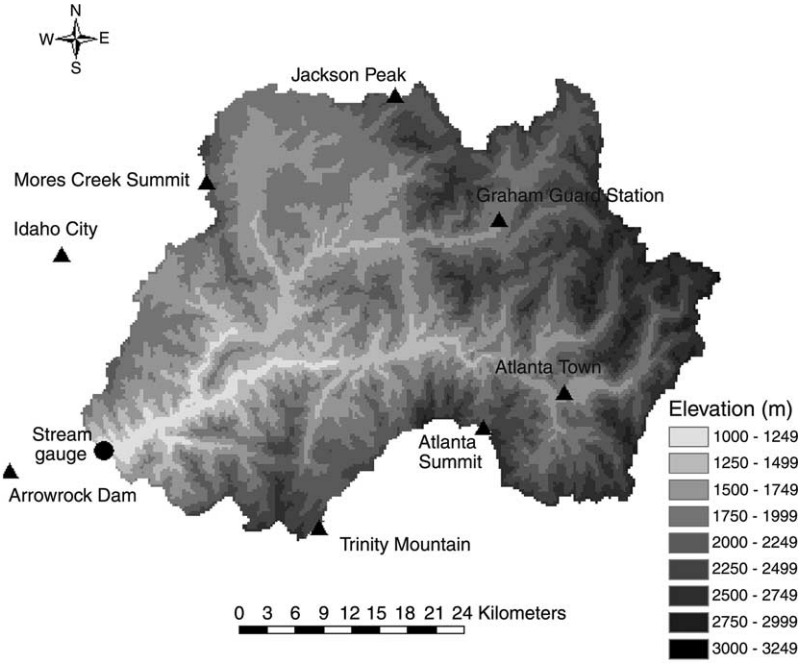

Fig. 1. Boise River basin and data sites.

Table 1
Meteorological station characteristics

Station name	Elev. (m)	Lat. (d–m–s)	Long. (d–m–s)	Variables measured
Arrowrock Dam	1070	43–36–40	115–55–19	p, t
Idaho City	1219	43–50–10	115–50–05	p, t
Atlanta Town	1649	43–48–15	115–08–35	p, swe, t
Graham Guard Station	1764	43–57–14	115–16–26	p, rh, sd, smt, sr, swe, t, w
Mores Creek Summit	1883	43–55–55	115–39–56	p, swe, t
Jackson Peak	2131	44–03–03	115–26–36	p, rh, sd, smt, sr, swe, t, tr, w
Atlanta Summit	2338	43–45–23	115–14–20	p, rh, sd, smt, sr, swe, w
Trinity Mountain	2377	43–37–43	115–26–16	p, swe, t

Variable abbreviations: p, precipitation; rh, relative humidity; sd, snow depth; smt, soil moisture and temperature; sr, solar radiation; swe, snow water equivalent; t, air temperature; tr, thermal radiation; w, wind speed and direction.

the Boise airport, located approximately 90 km southwest from the centroid of the basin.

A digital elevation model (DEM) with a 250 m resolution was used for the primary characterization of the basin. At this resolution there are 34,412 grid cells within the drainage area. Although this is slightly larger than the fractal scale of most of the Earth's topography (Dubayah et al., 1989), and some important finer scale, topographically controlled snowcover and snowmelt processes will not be represented at this resolution, it does provide a good compromise between representing the terrain structure and having a manageable number of cells from a computational and data storage point of view.

A detailed digital vegetation map at a 30 m resolution was available from the US Forest Service, which was generalized and aggregated to a 250 m resolution to match the DEM grid. The vegetation grid was used in the snow modelling primarily to identify forested grid cells for making adjustments to solar and thermal radiation. For subsequent water balance modelling, it was used to assign parameter values for rooting depth, leaf area index, and interception storage capacity.

Table 2
Snowmelt model runs

	1998	1999	2000
Start day	9 October 1997	5 November 1998	17 November 1999
End day	25 August 1998	17 August 1999	31 July 2000
Run duration (days)	321	286	258
Execution time (h:m)	23:41	18:38	17:08
Size of input files (MB)	1154.5	986.2	874.3
Size of output files (MB)[a]	424.9	378.4	341.2

[a] Size of output files is for daily output. This would be substantially larger if output were produced more frequently.

Model runs with *isnobal*, using input spatial fields of precipitation, air temperature, dew point temperature, wind speed, net solar radiation, and incoming thermal radiation, were made for three water years, 1998–2000 (water years begin on 1 October of the previous year). They were begun at the first snowfall and ended when most of the snow had melted. Table 2 gives the beginning and ending dates of each run along with the execution time and the disk storage required for all input and output files. The model output consists of spatial fields of all energy and mass fluxes and state variables. These results were stored once per day. The model runs were carried out on a Sun Ultra 10 workstation.

3. Description of snow model

The energy and water fluxes simulated by the *isnobal* model are depicted in Fig. 2 and are described in detail by Marks et al. (1998, 1999b) and Link and Marks (1999a). The surface snow layer is where all of the energy exchanges with the atmosphere occur; these processes do not penetrate very far, so the thickness of this layer is set at a value of 0.25 m in the model after the work of Link and Marks (1999b). The lower layer is simply the remainder of the snow cover. Both layers are assumed to be homogeneous and are characterized by their average temperature, density, and liquid water content. The model assumes that energy is transferred between the surface layer and

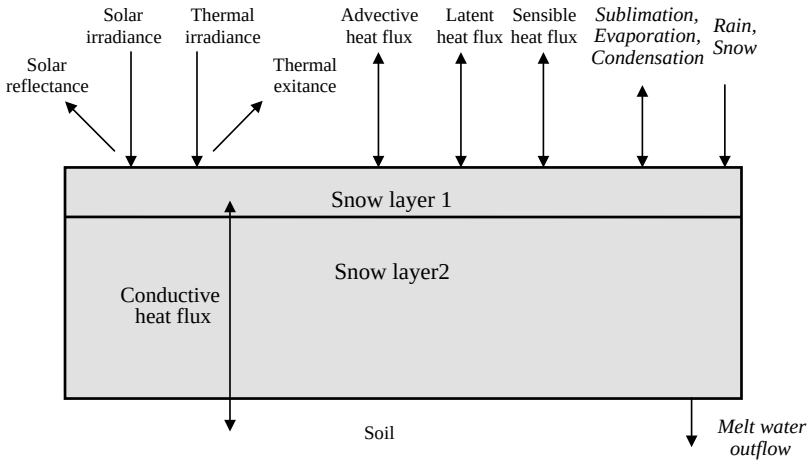

Fig. 2. Diagram of snow model components (energy fluxes in normal type, water fluxes in italics).

the lower layer and between the lower layer and the soil by conduction and diffusion. At each time step, the model computes the energy balance and the snow surface temperature and then adjusts the temperature and specific mass of each layer. If the computed energy balance is negative, the cold content, or the energy required to bring the temperature of the snowcover to 0 °C, is increased, and the layer temperature decreases. If the energy balance is positive, the layer cold content is decreased until it is zero. Additional input of energy causes the model to predict melt. If melt occurs, it is assumed to displace air in the snowcover, causing densification and increasing the average liquid water content of both layers. Liquid water in excess of a specified threshold becomes predicted outflow from the snowpack. The thickness of the surface layer remains constant until the lower layer is completely melted, at which time the model treats the snowcover as a single layer.

4. Spatial field time series of meteorological input data

A prerequisite for any model is to provide it with the best input data as is reasonably possible. If these data are of poor quality, then the entire hydrologic simulation is flawed from the outset. Given reliable input data, however, it has been shown that the development and melting of the seasonal snowcover can be accurately simulated (Susong et al., 1999).

Particularly in mountainous areas, where complex interactions among topography, vegetation canopies, and climate exist, it is essential that spatial interpolation methods that account for these effects be applied to estimate the spatial fields of meteorological input. In this paper, we show how a combination of limited measurements, models, and carefully applied spatial interpolation methods can be used to develop the spatial field time series of the forcing data required for the simulation of the development and melting of the seasonal snowcover.

The meteorological input to a spatially distributed energy balance snowmelt model includes spatial field time series of precipitation, air temperature, dew point temperature, wind speed, and solar and thermal radiation. These variables have particular characteristics and levels of data availability that make it necessary to use a variety of procedures to develop spatial fields of each. It is also essential to consider the effects of the forest canopy on the solar and thermal radiation.

Many areas do not have all of the measurements necessary for energy balance modelling. This is particularly true for solar and thermal radiation, humidity, and wind speed. The Natural Resources Conservation Service (NRCS) of the US Department of Agriculture collects basic meteorological data (precipitation, temperature, and snow water equivalent) at several hundred sites in mountainous regions of the western US with its SNOTEL system. Recently, additional parameters (snow depth, soil temperature

and moisture, solar and thermal radiation, wind speed, and humidity) are also being monitored at a number of sites (Abramovich and Pattee, 1999). One of the goals of the research presented in this paper is to demonstrate the use of these additional parameters.

In this section, the procedures that have been developed to estimate 3 h spatial field time series of these variables from the routinely available ground and upper air measurements at a 250 m resolution for the Boise River basin are described. We have striven to use spatial estimation procedures that are as straightforward as possible so that their use in a routine operational setting is feasible.

4.1. Precipitation

Due to the mountainous terrain and the prevalence of snowfall, reliable radar-based precipitation fields are unavailable, so spatial interpolation of the precipitation amounts measured at meteorological stations is the only option. Several spatial interpolation algorithms for estimating fields of precipitation (and other variables) have been reported in the literature, ranging from simple classical procedures such as Thiessen polygons to complex geostatistical and splining methods. These, to a greater or lesser extent, attempt to account for horizontal variability and the influence of topographic and other geographic characteristics. In mountainous areas, where orographic influences are so important, simple procedures that do not consider such influences are inappropriate. Algorithms that explicitly or implicitly account for topographic and other characteristics must be used.

An interpolation algorithm should be physically understandable, parsimonious, and appropriate to the data available, the geographic and climatic characteristics of the area involved, and the spatial scale. In this case, mesoscale basins (i.e. between about 100 and 10,000 km^2) are targeted, in which typically there may be data available from only a few up to perhaps 20 meteorological stations. This is a smaller spatial scale than some of the models reported in the literature, such as the regional model PRISM (Daly et al., 1994; Daly et al., 2000) and the models tested by Jarvis and Stuart (2001a,b), which account for many topographic characteristics besides elevation. At the mesoscale, there are typically too few meteorological stations to define the influence of topographic characteristics other than elevation. (This is likely not to be a significant restriction anyway because, as Jarvis and Stuart (2001b) suggest, it may not be necessary to add additional explanatory variables, as the spatial coherence can be exploited to compensate for lack of knowledge of secondary physical effects.)

After reviewing many procedures, Garen et al. (1994) decided upon elevationally detrended kriging as being the most appropriate for this purpose. It is fairly straightforward, and the elevation trends are explicitly represented (in contrast to other kriging variations, such as cokriging and external drift kriging, which are more complex and deal with the trend in an implicit fashion (Phillips et al., 1992; Hudson and Wackernagel, 1994)). We prefer detrended kriging because of its straightforwardness, clear physical interpretation, and complete control over the elevation trends. It was extensively tested using cross-validation techniques by Garen et al. (1994), and it has been successfully used in several hydrologic modelling studies (e.g. Susong et al., 1999; Geyer et al., 2001; Geyer and Schumann, 2001).

We give here a brief explanation of the detrended kriging algorithm; see Garen et al. (1994) and Garen (1995) for more details. The method is fairly simple in concept, dividing the variability into a vertical and a horizontal component. The vertical component is described by linear precipitation–elevation regressions (using least absolute errors, for robustness), estimated separately for each day to capture the time-varying orographic effect. The residuals from this linear trend are computed for each meteorological station, which are then subjected to ordinary kriging to compute spatial fields of residuals, thus describing the horizontal component of the variability. To obtain the final precipitation estimate at each grid cell, the kriged residual is added to the linear trend based on the elevation of the grid cell.

The concept behind the ordinary kriging part of this procedure is that the deviations from the overall precipitation–elevation relationship should show spatial coherence. This means, then, that if a meteorological station has a positive residual, the grid cells in its vicinity should also have a positive residual, and likewise for negative residuals. The spatial coherence is represented by the semivariogram.

In this work, a linear semivariogram is assumed throughout; at this spatial and temporal scale, little flattening of the semivariogram with separation distance occurs because the distances within the basin are less than the range of the semivariogram. The linear form simplifies the computations because the station weights from the kriging algorithm are then independent of the slope and intercept of the semivariogram and are, therefore, time-invariant.

On days when the slope of the linear precipitation–elevation trend is statistically insignificant, a zero trend is assumed, and the interpolation consists of only kriging in the horizontal. This is also done on (rare) days when the trend slope is negative, because the procedure is conceived only to handle the usual orographic increase of precipitation with elevation.

Fig. 3 shows an example of the detrending and the estimated daily precipitation field for a day with

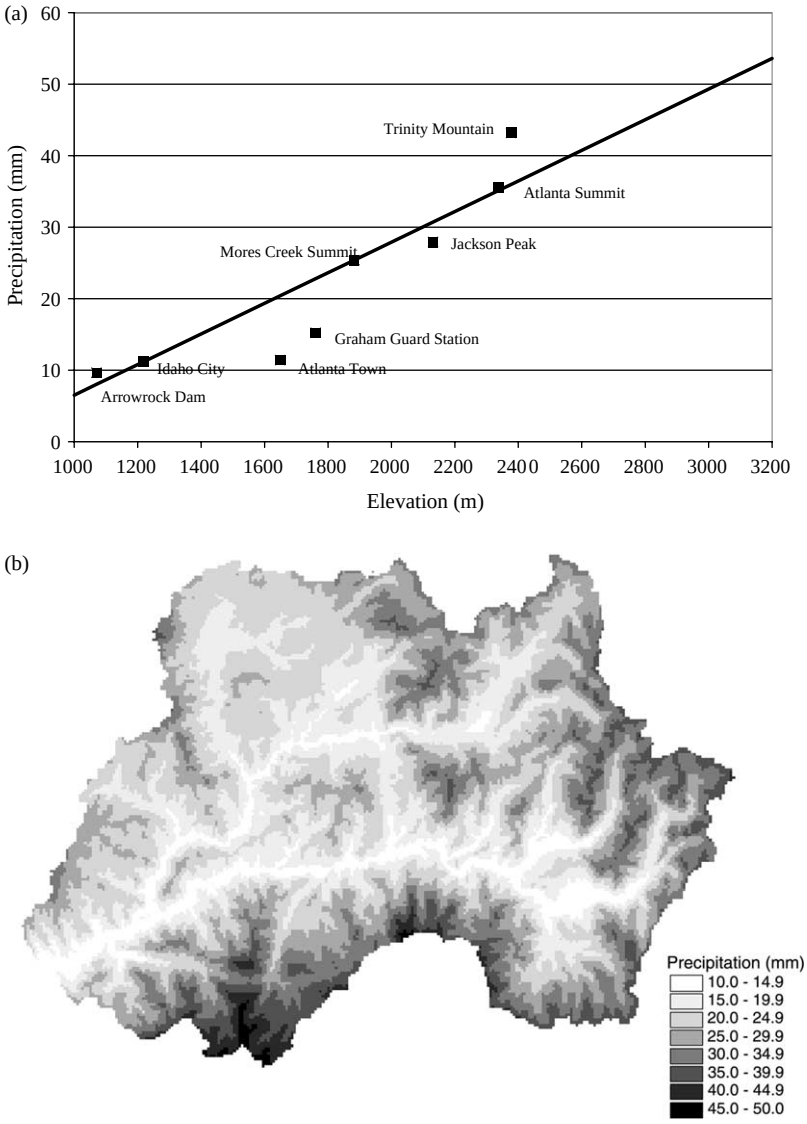

Fig. 3. (a) Precipitation–elevation relationship for 21 February 1998; (b) daily precipitation field resulting from detrended kriging interpolation.

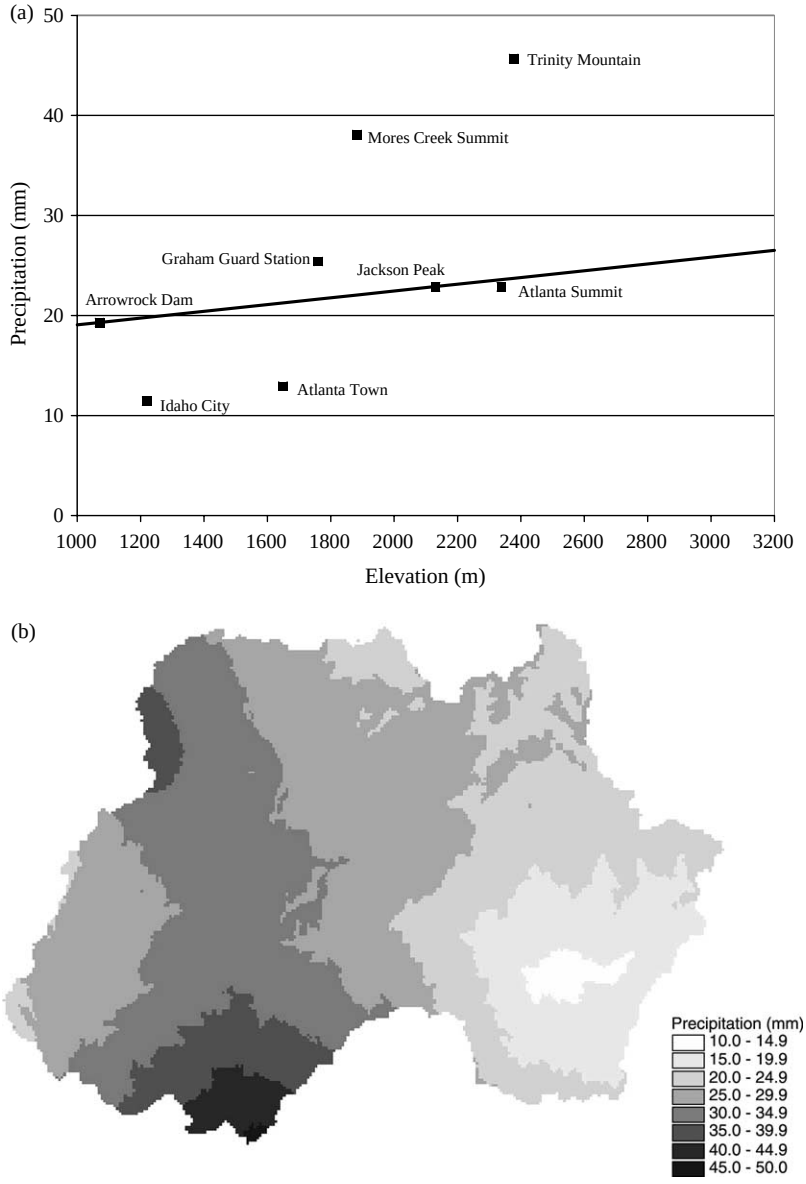

Fig. 4. (a) Precipitation–elevation relationship for 22 March 1998; (b) daily precipitation field resulting from detrended kriging interpolation.

significant precipitation and a strong precipitation–elevation relationship. Fig. 4 shows an example with similar amounts of precipitation but with a much weaker precipitation–elevation relationship. The different spatial patterns can be clearly seen. Fig. 3(b) shows a pattern closely following the elevation (Fig. 1), with only slight variations, such as the area of relatively high precipitation around the Trinity Mountain site in the southwest part of the basin. Fig. 4(b) shows little correspondence to the elevation pattern and reflects much more the spatial pattern of the individual stations alone. The dramatic difference in these precipitation–elevation trends underscores the need to use time-varying trends and not to rely on climatological averages, or trends for highly aggregated time periods such as months

(the latter point also noted by Hay et al. (1998)). Note, however, that there can be considerable uncertainty in estimating the elevation trends when the data are highly scattered, as in Fig. 4. Note also that the precipitation–elevation trend must be extrapolated a significant distance above the highest station elevation (2377 m) to the maximum elevation of the basin (3135 m), which is another possible source of uncertainty for the estimated fields and an indication of the need for additional meteorological stations.

Measuring precipitation in mountainous areas is difficult, and the data tend to be noisy. This is manageable at a daily time scale but not at sub-daily time scales, where the fluctuations are often too great to obtain an accurate measure of the within-day distribution of precipitation. It was decided, then, not to try to use the sub-daily (3 h in this case) data directly but rather to interpolate the daily fields, then disaggregate them to obtain the 3 h fields. A fractioning approach was adopted in which a single set of eight fractions for each day was multiplied with the respective daily precipitation field to obtain eight 3 h fields. The sets of fractions for each day were obtained by first computing fractions for each meteorological station (3 h amounts divided by daily total) and subjectively editing and smoothing these to remove the fluctuations due to noise. Then, the sets of fractions for all of the stations were averaged to obtain the final basin-wide set for the day. It was found that on days with significant amounts of precipitation, the 3 h fractions were fairly consistent among the stations, as would be expected with winter frontal-type storms. On days with small amounts of precipitation, the occurrence tended to be spotty, and the fractions varied considerably. This, however, matters little in terms of estimating the precipitation fields for snow modelling, and when it does matter (i.e. during the significant precipitation events), the distribution throughout the day could be estimated reasonably well.

4.2. Temperature

The elevationally detrended kriging procedure described above was also applied to temperature data, with minor variations. Since temperature data are more stable and less noisy than precipitation data, the 3 h temperature fields were estimated directly from the 3 h data rather than using any kind of disaggregation procedure as for precipitation. Also, only negative trend slopes are allowed, representing the normal cooling with elevation, otherwise a zero trend is assumed, in which case the interpolation consists of only kriging in the horizontal. This can lead to some interpolation inaccuracies, particularly in winter when cold air pockets and temperature inversions distort the overall temperature–elevation relationship. This, however, is believed not to cause serious errors in the energy balance of the snowpack because temperatures are already well below freezing, and likewise it will not lead to significant errors in computing snow evaporation, which already is basically zero under these conditions.

Fig. 5 gives an example of a temperature–elevation relationship along with the resulting spatial field. Stronger relationships typically occur in midday (shown in Fig. 5), while weaker ones, when they occur, are generally at night and early morning. As with precipitation, it is important to use the data for each time period to estimate the temperature–elevation relationships, since adiabatic lapse rates, and average elevational trends (e.g. Wigmosta et al., 1994; United States Army Corps of Engineers, 1987; Anderson, 1973) often do not adequately represent the actual trend for any given time period.

4.3. Dew point temperature/vapor pressure

Dew point temperature and vapor pressure are considered together because they have a one-to-one correspondence, and they both relate to the humidity of the air. They are used in *isnobal* for two main purposes. The dew point temperature is used as a surrogate for the temperature of the precipitation, while the vapor pressure is used in computing the latent heat flux into or out of the snowpack. These quantities determine the form of precipitation (solid or liquid) as well as the condensing/evaporating conditions of the snowpack.

Dew point temperature and vapor pressure are computed from air temperature and relative humidity. Since only three stations in the Boise basin have relative humidity sensors, an interpolation procedure such as that used for precipitation and temperature cannot be applied. Instead, a simple elevation-based procedure was used. The stations with relative

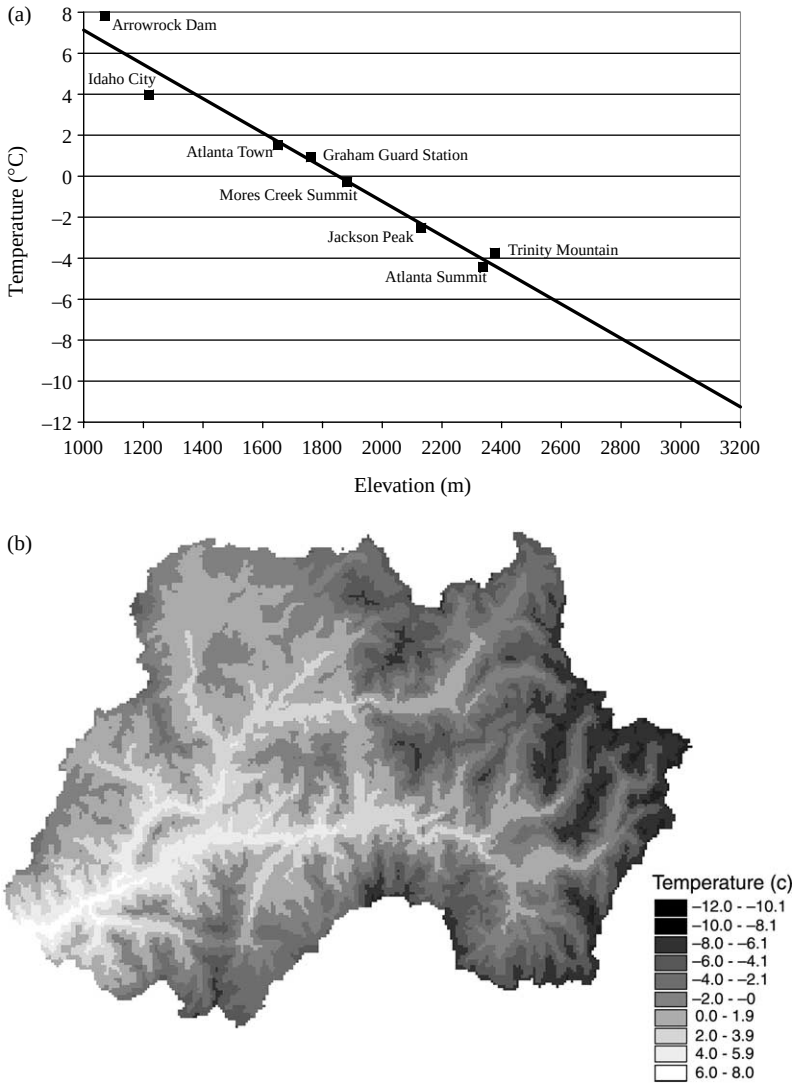

Fig. 5. (a) Temperature–elevation relationship for 21 February 1998, 1200–1500; (b) temperature field resulting from detrended kriging interpolation.

humidity sensors are, unfortunately, clustered around the middle of the elevation range of the basin, making it impossible to estimate any kind of meaningful trend with elevation. Instead, the 3 h air temperature-relative humidity pairs for each station were converted to vapor pressure, then these values for the three stations were averaged and assumed to be applicable at 2100 m, an approximate mean of the three station elevations. This mean vapor pressure was then converted to dew point temperature, representing one point on a dew point-elevation profile for the time period.

To fill out the profile, twice-per-day upper air soundings from the Boise airport (elevation 874 m) were used. The assumptions of this approach are first that the observed/averaged dew point (as obtained above) and the dew point at the surface level from the upper air profile can be used to represent the (linear) variation of dew point with elevation up to 2100 m. Second, above this elevation, the dew point should

gradually become that of the free atmosphere, as measured in the upper air sounding. To represent this, the difference between the observed/averaged dew point at 2100 m and the upper air dew point at this elevation was used as an initial 'offset' from the upper air profile. This offset was then linearly ramped to zero at 2800 m (above which are only the highest peaks), so that at this point and upwards, the dew point profile became that of the upper air profile.

With these assumptions, data, and some interpolation in time and elevation, dew point-elevation profiles were constructed at 100 m elevation intervals for each 3 h period. The derived dew point profiles were then applied to the DEM to obtain initial 3 h dew point fields. These had to be checked, however, to ensure that the estimated dew point was less than or equal to the interpolated air temperature for each grid cell; if not, it was made equal to the air temperature. A second check was made to ensure that the dew point was not greatly less than the air temperature if precipitation was occurring because we would expect that the relative humidity is high during rain or snowfall. If greater than 2 mm of precipitation occurred for the 3 h period for the grid cell, and if the initial estimate of the dew point was less than the air temperature by more than 0.5 °C, then the dew point was set equal to the air temperature minus 0.5°.

Fig. 6(a) shows an example of an estimated dew point-elevation profile together with the upper air soundings surrounding it in time. Fig. 6(b) shows the resulting dew point field using this profile after making the checks and adjustments. Once the final dew point fields were obtained, the vapor pressure fields were calculated directly from them.

4.4. Wind speed

Wind speed sensors are located at the same three stations that have relative humidity. These sensors report maximum and average wind speed at a 3 h time step. For the same reasons as for dew point temperature, a simplified interpolation procedure had to be developed to estimate 3 h wind speed fields. With wind, however, it is not possible to place as much reliance on upper air soundings as with dew point. Surface wind speed at the Boise airport cannot be taken as representative of surface wind speeds in the Boise River basin because of the great spatial variability of wind and because the terrain around the airport is flat and open, unlike that of the river basin. It is also expected that the wind speeds in the upper air soundings are significantly higher than what occurs at the ground surface due to the influence of the terrain.

With these thoughts in mind, an elevation-based procedure, along the lines of that used for dew point, was developed. The first step was to compute an average wind speed from the three observations available for each 3 h time period, which were considered to be representative for all elevations up to 2100 m. Physical reasoning suggests that the wind speed should increase with elevation, especially in the upper parts of the basin, where the terrain and vegetation have a declining effect on the overall wind pattern. An examination of wind speeds at 2100 and 3300 m from the upper air soundings showed that there is an average increase of a factor of 1.3–1.5 between these two elevations in the free atmosphere. Using this as a guide, the second section of the wind speed-elevation profile consisted of the observed/averaged value at 2100 m with a linear increase up to a value 1.5 times this at 3300 m (just above the highest elevations in the basin). This simple two-section wind speed-elevation profile for each 3 h period was applied to the DEM to obtain initial wind fields. For non-forested grid cells, the initial wind speed values were multiplied by 1.5 to represent the expected higher wind speeds in open areas as opposed to forested areas. The multiplier 1.5 is smaller than the 3.5 multiplier reported by Link and Marks (1999b) for open forests in Boreal Canada but was chosen based on our judgment, since the wind measurements in the Boise River basin were made in forest clearings rather than directly below the forest canopy.

4.5. Solar radiation

Determining the solar radiation input to the snowpack was the most difficult and complex part of the data preparation effort. This involved a multi-step procedure of data analysis and modelling, and many issues had to be resolved. The procedure uses a model to compute terrain-corrected clear sky incoming solar radiation, uses measurements to estimate a reduction for cloud cover, and then subtracts modelled reflected radiation. The end result is a spatial field time series of net solar radiation, which is required as input to

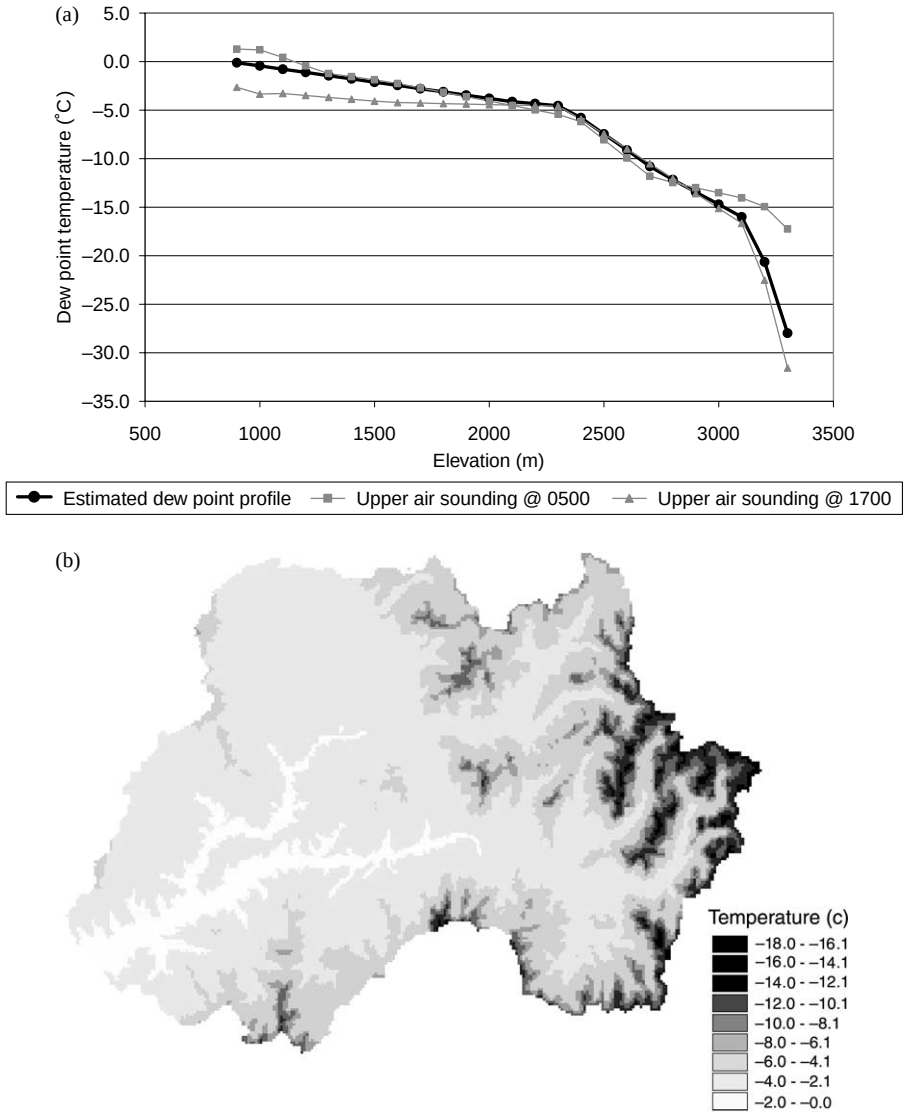

Fig. 6. (a) Dew point temperature profiles from upper air soundings on 20 April 1998 and as interpolated for the time period 1200–1500; (b) dew point temperature field resulting from interpolated profile, after checks and adjustments.

the *isnobal* model. The issues and processing steps are described below.

4.5.1. Instruments and data

Solar radiation sensors were installed at the three enhanced SNOTEL sites that also have relative humidity and wind speed sensors. All three sites were equipped with a standard, relatively inexpensive instrument (made by the Matrix company in AZ, USA). The Jackson Peak site was also equipped with three laboratory-quality instruments (made by the Eppley company in RI, USA)—a clear filtered solar pyranometer (measuring wavelengths 0.28–2.8 μm), a red filtered solar pyranometer (measuring wavelengths 0.7–2.8 μm, that is, the near infrared part of the solar spectrum), and a pyrgeometer (measuring wavelengths 3.5–50 μm, that is, long-wave thermal radiation). All sensors were mounted on towers

approximately 7–9 m above ground level to minimize shadowing by the forest canopy.

The Eppley clear filtered pyranometer was installed to check and calibrate data from the Matrix radiometer. After examining the data, it became apparent that the Matrix instruments at Jackson Peak and Graham Guard Station were not functioning properly. It could not be determined whether the cause of this was instrument failure or a problem with the interface to the SNOTEL data logging system. Data from the Jackson Peak Eppley pyranometer were generally similar to data from the Atlanta Summit Matrix radiometer. Only the data from these two instruments were used for our analysis.

4.5.2. Data interpretation, solar radiation modelling, and cloud correction factor

The solar radiation fields used by Susong et al. (1999) were based entirely on simulated values. For the research reported here, we combined measured solar radiation with simulated values to develop the spatial field time series of radiation required for input to *isnobal*. The observations were used for two purposes, to calibrate the parameters of the solar radiation model and to estimate daily basin-wide cloud correction factors.

The IPW software package includes the detailed point radiation transfer model *twostream*, which can simulate clear sky spectral radiation transfer through a specified atmosphere for a chosen wavelength band. The *twostream* model was coupled with a DEM-based terrain shading and horizon model (Dozier and Frew, 1990) in the IPW utility *toporad*. This utility adjusts the *twostream* calculations for topographic effects such as slope, aspect, and shading from nearby terrain; a description and application of the model is given by Dubayah et al. (1990). Initial values of model parameters were taken from the literature, and they were fine-tuned by manual calibration with measured solar radiation data on clear days.

To estimate the incident solar radiation at the snow surface beneath a forest canopy, it is necessary to determine the direct beam/diffuse split in the incident solar radiation (Link and Marks, 1999a). Because data on direct beam and diffuse components of solar radiation were not available, the direct beam and diffuse components from *twostream* and *toporad* could not be independently verified. They are also only valid under clear sky conditions, therefore, another method, applicable for both clear and cloudy conditions and described in Section 4.5.5, was used to determine the direct beam/diffuse split.

The red filtered Eppley pyranometer was used to measure the near infrared part of the solar spectrum to ensure that the solar radiation model simulated the correct fraction of the total in this wavelength band. It is important to have the visible (0.28–0.7 μm) and the near infrared (0.7–2.8 μm) portions of the solar spectrum correctly characterized because the albedo of snow is very different for these two wavebands (Warren and Wiscombe, 1980; Wiscombe and Warren, 1980). Comparisons of measured and modelled total and near infrared radiation showed that the observed near infrared fraction was well simulated by the model.

Using the calibrated model parameters, an entire annual cycle of clear sky solar radiation was simulated for the Jackson Peak and Atlanta Summit sites with *twostream*. The ratio of observed to simulated radiation was then computed for each time period for each site. Because there appeared to be morning and evening shadowing of the instruments, only the ratios for the periods 0900–1200 and 1200–1500 were meaningful, and they were combined into a single ratio. The ratios for the two sites were then averaged, representing the cloud correction factor, which was applied to all time periods of the day. For simplicity, and to keep the procedure applicable to basins without near infrared measurements, the same cloud cover correction ratio was used for both the visible and infrared wavebands.

4.5.3. Snow albedo

The albedo of clean snow declines with time after it is deposited due to grain growth and contamination. The rate of albedo decay is likely to vary spatially as a function of topography and canopy cover, as was shown by Molotch et al. (2004). For this study, however, albedo decay was considered uniform over the basin as function of time since the last storm and was modelled using the IPW utility *ialbedo*, which is based on the work of Marshall and Warren (1987) and Marks (1988). The visible and near infrared albedoes are modelled separately. In general, the simulated visible albedo starts out above 0.98 and decays with age down to around 0.9, while the simulated near

infrared albedo starts at approximately 0.75 and decays down to about 0.4.

The albedo modelling was done as part of the net radiation calculations, which were carried out as a preprocessing step that prepared the spatial field time series of net solar radiation required for input to the *isnobal* model. In these calculations, clear sky visible and near infrared solar radiation fields were calculated first, then the cloud cover correction was applied to both, after which the albedoes for each wavelength band were calculated and the reflected solar radiation subtracted to obtain net radiation. Snow events had to be defined a priori by examining the precipitation, temperature, humidity, and snow water equivalent data from the meteorological stations. Using these data, it was straightforward identifying days during which snow fell. Initial and maximum grain size parameter values were computed using guidance from the IPW documentation for the *albedo* and *ialbedo* utilities and prior experience from Marks et al. (1999b), based on the air and dew point temperatures at the meteorological stations. The contamination parameter was set to a constant value representing clean, uncontaminated snow, as would be expected in this remote mountainous area.

4.5.4. Albedo reduction for surface debris

In areas of coniferous forest, debris such as needles and twigs are dropped continuously onto the snow surface. During the winter, new snowfalls cover this debris, so the effect of the debris on the snow albedo is small. In the spring, however, as melt is underway, this debris, which has been incorporated into the snowpack, is exposed and collects on the surface of the snow. This accumulation of exposed debris can substantially decrease the albedo, thus increasing the absorption of solar radiation and affecting the rate of snowmelt (Link and Marks, 1999b; Hardy et al., 2000; Melloh et al., 2001). This represents an albedo reduction in addition to the decrease with aging and grain growth modelled by *ialbedo*, and it must be represented in the net radiation computations.

The procedure to account for the reduction of albedo due to surface debris was based on computing a reduction of the clean snow albedo beginning with the onset of melt, reducing it to approximately half its modelled value by final melt out. This reduction is in line with that reported by Link and Marks (1999b) and suggested by Melloh et al. (2001).

A square root model was used for the albedo reduction for surface debris:

$$R = \alpha \sqrt{\frac{D_c - D_p}{D_m - D_p}} \tag{1}$$

where R = albedo reduction (to be subtracted from the *ialbedo* computed value), α = maximum albedo reduction (set to 0.5 for both visible and infrared), D_c = current Julian date, D_p = peak snow water equivalent Julian date for current year, and D_m = melt out Julian date for current year. This correction is applied only during the melt period. The nonlinear functional form gives albedo reductions that increase rapidly at first then level off, as supported by the work of Hardy et al. (2000) and Melloh et al. (2001). To ensure that these reductions did not result in physically unreasonable albedo values, lower bounds of 0.4 for visible and 0.2 for infrared albedoes were applied.

To implement this concept spatially required the evaluation of the date of peak snow water equivalent and the date of melt out to define the snowmelt period for which the albedo reduction for surface debris was to be applied. For each of the 3 years simulated, separate linear regressions of these two dates with elevation for all of the sites with snow water equivalent data were calculated and applied to the DEM grid to obtain spatial fields of peak snow water equivalent and melt out dates.

The concept behind this albedo reduction due to the deposition of debris on the snow surface was originally envisioned as occurring only in forested areas. Preliminary simulations and results reported by Melloh et al. (2001) showed, however, that some debris is also deposited in adjacent non-forested areas. To represent this, the albedo reduction for surface debris in non-forested grid cells was set at half of the reduction in forested grid cells.

Fig. 7 shows the progression of modelled snow albedo for the Jackson Peak site (a forested location) during the 1998 melt season both with and without the albedo reduction for surface debris. The difference between the visible and infrared wavebands and the occurrence of snow events are clearly seen.

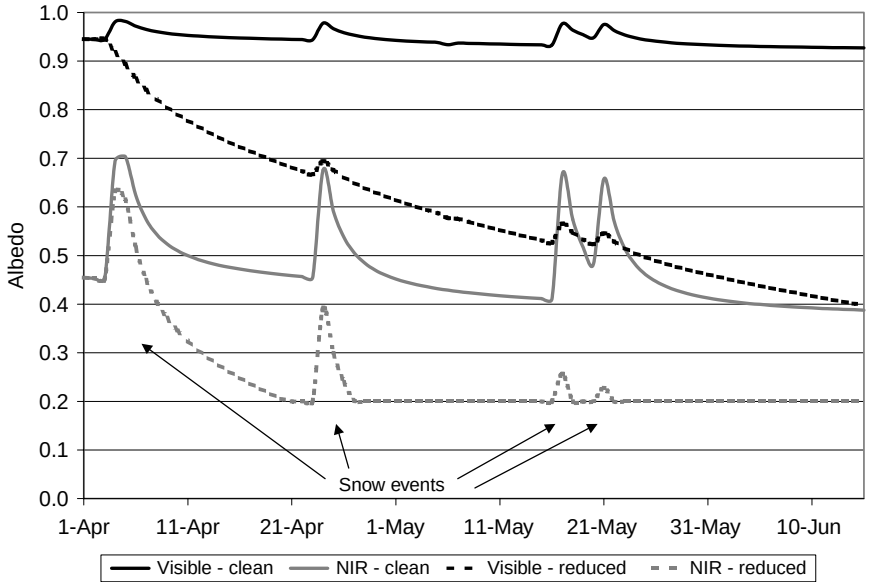

Fig. 7. Snow albedo for 1998 snowmelt season at Jackson Peak, showing values for clean snow and with albedo reduction for surface debris for visible and near infrared (NIR) wavebands. Albedo reduction for surface debris begins on 4 April, the day after peak snow water equivalent at this site for this year. If Jackson Peak were unforested, the reduced albedo traces would lie halfway between the clean and reduced traces shown here.

4.5.5. Direct beam/diffuse split

The forest canopy corrections (described in the next section) require the differentiation of the solar radiation into direct beam and diffuse components. Although *toporad* produces images of direct and diffuse radiation, the model is only appropriate for non-cloudy skies. A method had to be found that could take the total radiation from the cloud-corrected *toporad* output and split it into direct and diffuse components.

Though satellite data have been used to estimate the distribution of cloud cover (Dubayah and Loechel, 1997), that was beyond the scope of this study. Several surface data-driven procedures reported in the literature were investigated to evaluate their behavior and assess their appropriateness for this application. These included procedures from Bristow et al. (1985), Gul et al. (1998), and University of Oregon (1999, Chapters X and XII), as well as the IPW utility *cf_cloud*. These procedures use various functional forms, but they can all be expressed as relating the transmission of total solar radiation through the atmosphere (including clouds) to the transmission of the direct and diffuse components. Although there were not great differences in this split among the methods, the procedure of Bristow et al. (1985) was selected as behaving in the most reasonable and understandable fashion.

With a model parameter value that gives a small diffuse fraction (0.1) on clear days, as would be expected in this remote, high elevation area, the equation used by Bristow et al. (1985) to make the split becomes

$$F_d = 1 - e^{1-(1/T)} \quad (2)$$

where F_d = fraction of total radiation reaching the ground that is diffuse and T = total transmissivity (ratio of extraterrestrial radiation to that received at the ground). The diffuse radiation is then computed by multiplying the total by this fraction, and the direct radiation is simply the total minus the diffuse.

4.5.6. Forest canopy corrections

Trees exert a significant effect on the solar radiation reaching the snowpack beneath. For forested grid cells, the incoming solar radiation was modified according to the canopy corrections developed by Link and Marks (1999a) for the Boreal forest. These

corrections were applied in the same way both to the visible and infrared wavebands.

For direct beam radiation, the following correction is made:

$$R_{bc} = R_b \, e^{-\mu h/\cos\theta} \quad (3)$$

where R_{bc} = corrected (i.e. beneath the forest canopy) direct beam radiation, R_b = direct beam radiation above the forest canopy, μ = extinction coefficient, h = canopy height (m), and θ = solar zenith angle.

For diffuse radiation, the following correction is made:

$$R_{dc} = \tau R_d \quad (4)$$

where R_{dc} = corrected (i.e. beneath the forest canopy) diffuse radiation, R_d = diffuse radiation above the forest canopy, and τ = transmissivity.

Values of the two parameters, μ and τ, are given by Link and Marks (1999a) for different classes of forest type and density. Based on some test point simulations with *snobal*, the parameter values assigned differed slightly from the values given by Link and Marks (1999a), probably because the forests in the Boise River basin are more open than the Boreal forest. For the parameter μ, the values assigned were 0.016, 0.025, and 0.033 for deciduous forest, mixed forest, and coniferous forest, respectively, which are a little smaller than those given by Link and Marks (1999a). For the parameter τ, the values assigned to the three forest types were 0.60, 0.44, and 0.30, respectively, which are a little higher than those given by Link and Marks (1999a). A canopy height of 10 m was used for all forest types.

4.5.7. Net solar radiation calculations

All of above algorithms and processing steps were programmed into a UNIX script, executing the appropriate IPW utilities and performing calculations on the spatial fields. The script was programmed to simulate a given day using parameters (cloud correction factor, snow albedo parameters) applicable for the entire day. To capture the rapid diurnal changes in solar radiation with time and sun angles, a 20 min time step was used for the calculations, and the appropriate fields were averaged to obtain 3 h spatial fields required by *isnobal*. A flowchart of the processing steps is given in Fig. 8.

4.6. Thermal radiation

Thermal radiation, sometimes also called longwave or infrared radiation, is emitted by the atmosphere, clouds, and trees, and this is a significant energy input to the snowpack. The *isnobal* model requires incoming thermal radiation as input and computes the outgoing thermal radiation emitted by the snowpack. The steps used to compute 3 h spatial field time series of incoming thermal radiation are described below.

4.6.1. Clear sky thermal radiation

The IPW utility *topotherm* calculates clear sky thermal radiation emitted by the atmosphere over a DEM grid. The model represented by the *topotherm* utility was developed by Marks and Dozier (1979) and is based on air temperature, dew point temperature, elevation, and topographic characteristics. It estimates an effective emissivity for the atmosphere so that incoming thermal radiation can be calculated from near-surface air temperature. Because thermal radiation does not depend on sunrise and sunset times or solar angles, it is unnecessary to use a small computational time step as with solar radiation. The *topotherm* utility was, therefore, executed using the 3 h air and dew point temperature fields described earlier directly as input.

4.6.2. Cloud correction

Cloud cover increases the effective emissivity of the atmosphere, increasing the input of thermal radiation at the surface. While the effective atmospheric emissivity during clear sky conditions may range from 0.60 to 0.75, cloud cover may increase this to close to 1.0. Although Marks and Dozier (1979) showed that clear sky thermal radiation fields could be effectively simulated, accounting for cloud effects requires thermal radiation measurements. Such measurements from the Eppley pyrgeometer at the Jackson Peak site were used to develop a cloud correction factor to be multiplied with the clear sky fields computed with *topotherm*. Unfortunately, measured thermal radiation was not available for a significant portion of the modelled time period, requiring a method of estimating the cloud correction factors from other information.

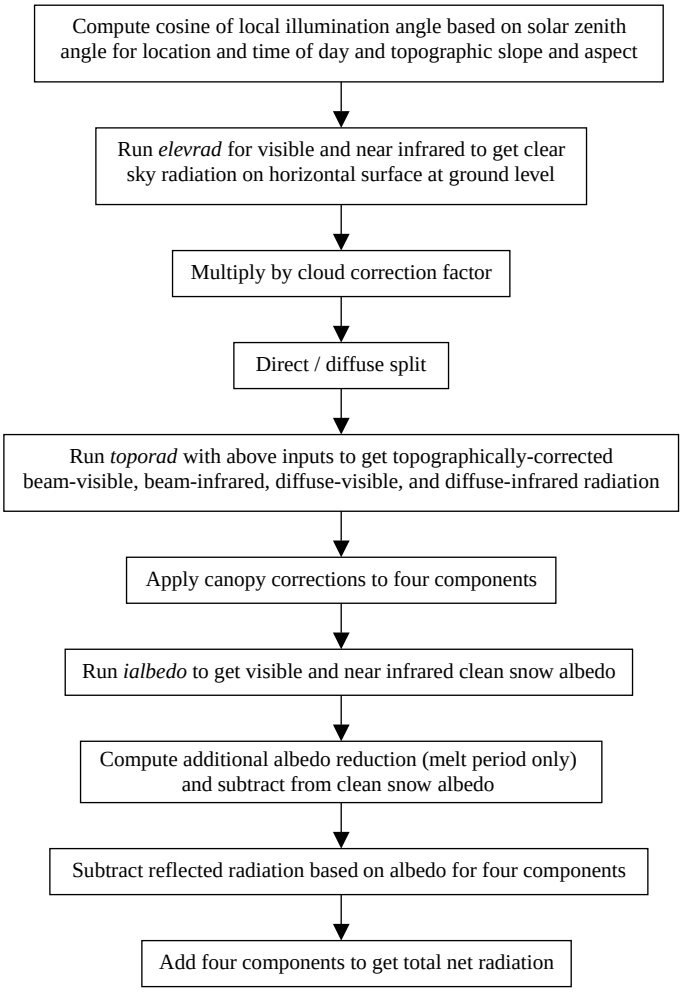

Fig. 8. Flowchart of net radiation calculations for each 20 min time step when the sun is up for each grid cell within the catchment (IPW utility names in italics).

The method developed is based on the idea that if the solar radiation ratio (measured to simulated clear sky) is high (near one), this would indicate that there are few clouds, and the thermal radiation ought to be near the clear sky value (ratio also near one). On the other hand, if the solar radiation ratio is low (much less than one), this would indicate a cloudy day, and the thermal radiation would be higher than modelled (ratio significantly greater than one). Using the ratio of measured to simulated solar radiation as an indicator of cloud cover, a relationship was developed between measured and simulated thermal and solar radiation over the period when both thermal and solar data were available. A linear regression was performed between the ratios of measured and simulated thermal and solar radiation, between the hours 0900 and 1500. The resulting equation was $\mathrm{TRR} = 1.485 - 0.488\mathrm{SRR}$, with $r^2 = 0.75$, where TRR = thermal radiation ratio and SRR = solar radiation ratio. With this relationship, it was possible to compute thermal ratios for all days. As with the solar ratio, the thermal ratio was applied to all time periods within a day. The

fact that TRR is near one when SRR is near one in this regression equation is additional verification that *topotherm* simulates reasonable clear sky thermal radiation values.

4.6.3. Forest canopy correction

Like cloud cover, a forest canopy increases the effective emissivity of the atmosphere/canopy hemisphere over the snow surface. Because the branches, needles, and leaves in the canopy have an emissivity approaching 1.0, the increase in thermal radiation below a canopy is a function of the density, structure, and temperature of the canopy. The approach to adjusting thermal radiation for forest canopy effects, taken from Link and Marks (1999a), is

$$TR_c = \tau TR + (1 - \tau)\varepsilon\sigma T^4 \quad (5)$$

where TR_c = corrected (i.e. beneath the forest canopy) thermal radiation, TR = thermal radiation above the forest canopy, τ = transmissivity (same as for diffuse solar radiation), ε = emissivity (0.96), σ = Stefan–Boltzmann constant (5.6697×10^{-8} W/m^2/K^4), and T = air temperature (K). The first term of the equation gives the amount of thermal radiation from the atmosphere (including clouds) that is transmitted through the canopy to the surface, and the second term gives the amount of thermal radiation emitted by the trees themselves, assuming that they are at the ambient air temperature. The net effect is usually that $TR_c > TR$. The temperatures used are 3 h values from the air temperature fields previously calculated. This correction is only done for forested grid cells.

5. Simulation results and verification

With the meteorological forcing fields estimated using the procedures described above, the *isnobal* model was run to simulate the accumulation and melt of the snowpack for 3 years, as shown in Table 2. One additional required input is soil temperature, which we set to a constant of 0 °C. In this environment, the soil temperature rarely goes much below 0 (confirmed with some limited soil temperature and snow pit data), so this assumption should not lead to any appreciable error in the energy balance.

Verifying a spatial model is difficult, and often any one method by itself is inadequate. We, therefore, verified the snowmelt model results in four different ways, all of which were very favorable. These are described below.

5.1. Snow water equivalent

One way to assess the snow model results is to compare observed snow water equivalent with simulated values for the grid cells in which the meteorological stations are located. Unfortunately, a strict comparison is not possible, for two reasons. First, the observations are essentially point measurements, taken by registering the pressure in fluid filled snow pillows that have a surface area of approximately 7 m^2. The simulated values, however, represent an average for the entire grid cell, which in this case is 62,500 m^2 (250 m square). The second problem is that the snow pillows are installed on a flat piece of ground, whereas the grid cells in general have a topographic slope and aspect; the solar radiation balance for the two is, therefore, not the same. Despite these issues, it is still meaningful to make these comparisons.

Fig. 9 shows the course of simulated and observed snow water equivalent values for the six meteorological sites with snow pillows for 1998; the other 2 years are similar in appearance. In general, the model reproduced the observations quite well for all 3 years. The accumulation period always tracked very closely, as one would expect, since no snowmelt is occurring during the winter. Once snowmelt begins, the correspondence is not quite as close, but this is, again, as one might expect. There are times during the snowmelt period when the simulated snow water equivalent tracks the observations very closely (e.g. Jackson Peak and Trinity Mountain in Fig. 9); other times, the snowmelt gets a bit off track at some point, then it parallels the observations (e.g. Atlanta Summit); sometimes the simulation gets off track but then returns to follow the observations closely again (e.g. Graham Guard Station and Mores Creek Summit). Despite the discrepancies, it is felt that this correspondence is quite good, especially considering the issues in making this comparison (mentioned above) and considering that the model inputs are not optimized for each of the stations but rather are somewhat regionalized according to the methods used to prepare the spatial fields of meteorological input.

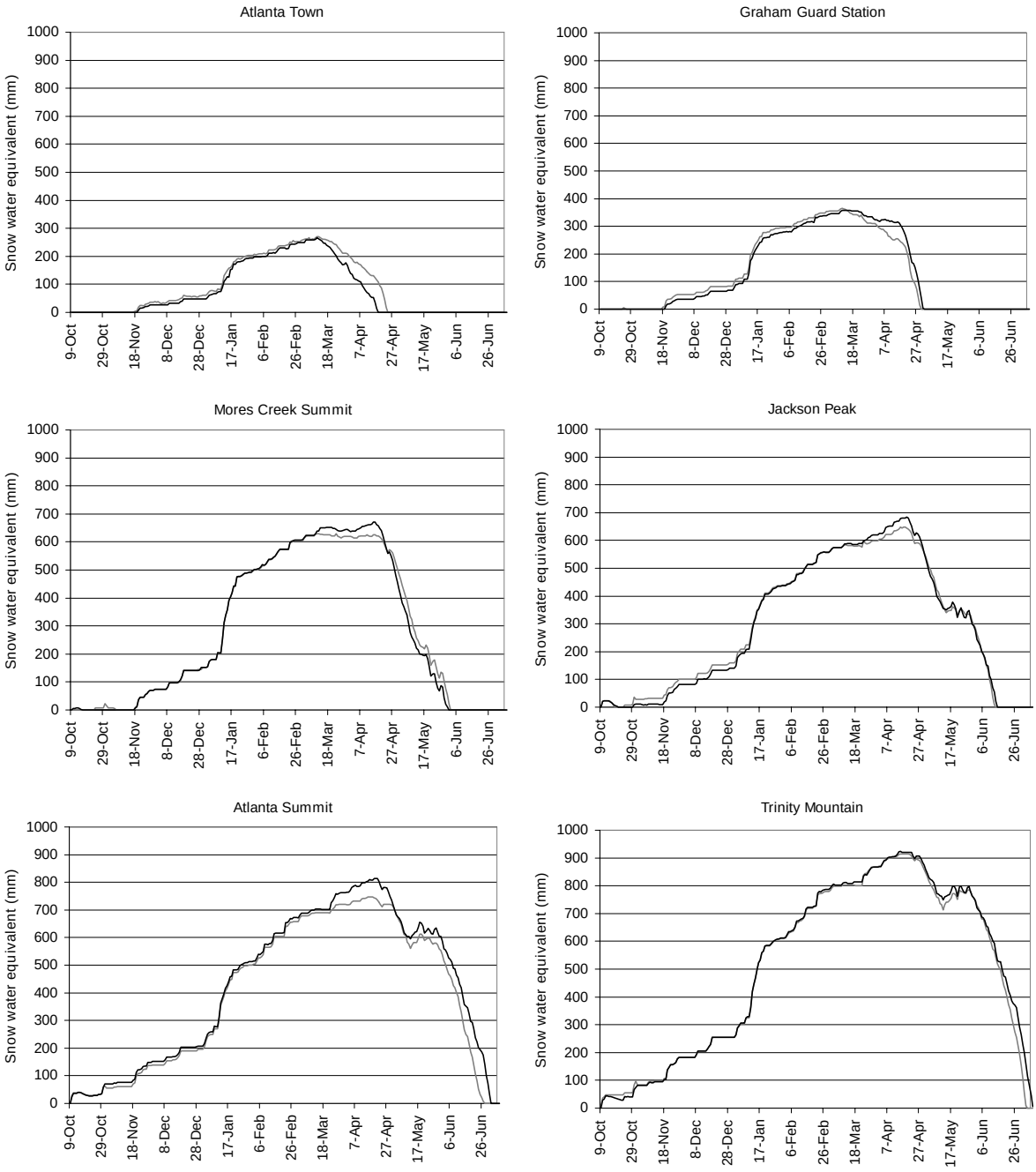

Fig. 9. Simulated (black) and observed (gray) snow water equivalent at meteorological stations, water year 1998.

5.2. Snow depth

Although comparing modelled with measured snow depth is not as useful for water resources purposes as snow water equivalent comparisons, it is still informative. Snow depth comparisons are a check on the representation of snow density within the model, and they can be of value in assessing

the potential of verifying the model in situations where only snow depth and not water equivalent data are available.

Three of the meteorological stations have ultrasonic snow depth sensors that take measurements directly over the snow pillows. Fig. 10 shows the course of simulated and observed snow depth values for these three meteorological sites for 1998. Snow depth is not as well simulated as snow water equivalent, but the results are still reasonably good. The simulated depths showed their greatest discrepancies during the period January–March, where Graham Guard Station tended to be undersimulated, and Jackson Peak and Atlanta Summit tended to be oversimulated. Since simulating the depth correctly is not as important as simulating the snow water equivalent, this somewhat poorer simulation for snow depth does not cause great concern.

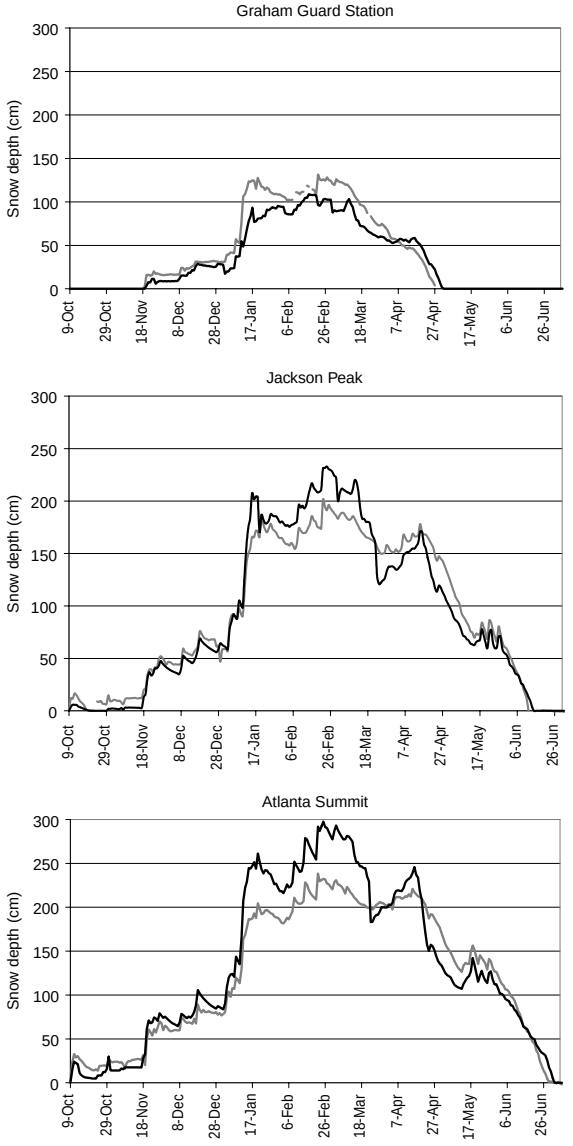

Fig. 10. Simulated (black) and observed (gray) snow depth at meteorological stations, water year 1998.

5.3. Snow covered area

Snow covered area images for the USA derived from satellite data are produced routinely by the National Operational Hydrologic Remote Sensing Center (NOHRSC) of the US National Weather Service (http://www.nohrsc.nws.gov). These images, which contain a snow/no snow binary classification of each grid cell, can be compared with the simulated snow covered area as a third method of model verification.

There are actually a few difficulties in doing this, so once again, this is not a completely fair comparison. The first issue is that the spatial resolution of the satellite images is coarser than that used here with the snowmelt model and that the map projections used are different. The NOHRSC images are in geographic coordinates (latitude–longitude) and have a spatial resolution of 30 arcsec. To be able to compare these images with the snowmelt model results, they had to be reprojected, resampled, and shifted so that the grid cells corresponded directly with those of the grid used for the snowmelt model. ARC/INFO was used to perform these manipulations. A simple reprojection of these images to the projection used for the Boise River DEM (Albers) resulted in a grid cell size of approximately 750 m. The ARC/INFO command *project* was used, then, not only to reproject to Albers but also to resample to 250 m. Small eastward and southward shifts were then required to achieve correct alignment. These manipulations of the NOHRSC images could lead to some inaccuracies in making comparisons with model results, the main issue being the difference in spatial resolution. Although sub-pixel estimates of snow covered area from AVHRR data similar to the NOHRSC data have been made (Rosenthal, 1996),

and there has been promising research on using new, higher resolution data from the EOS sensors to determine sub-pixel snow cover (Dozier and Painter, 2004), these approaches are beyond the scope of this study.

A second issue with the NOHRSC images is that it is difficult for the satellite to 'see' snow under a forest canopy. In preliminary comparisons of the satellite and simulated snow covered areas, the satellite values were usually significantly smaller than the simulated ones. It was suspected that in this region, where over half of the area is forested, the satellite had difficulty discerning snow under the trees, and this led to the low values. A simple adjustment was, therefore, made to the satellite values: for forested grid cells, if the satellite image indicated no snow and the snowmelt model indicated snow, this cell was added to the satellite snow covered area.

A third issue is that cloud cover makes many of the satellite images unusable. Only images with less than 5% of the basin under cloud were used in making comparisons. This meant that comparisons could only be made on a few days during the snowmelt season.

Fig. 11 shows a comparison of simulated and satellite snow covered area for the 1998, 1999, and 2000 snowmelt seasons. Also shown is snow covered area derived from snow pillow melt out dates. This was done as an additional very simple check on the simulated and satellite values. These snow covered area values were derived by first performing a linear regression of elevation versus melt out date for the meteorological stations with snow pillows then using this to predict a 'snow line' elevation for each day of the snowmelt season. This was used in conjunction with the DEM to compute the percent of basin area above this 'snow line'. This is a very crude estimate of snow covered area, but it was thought that it would provide one additional guideline in judging the simulation results, that is, they should be reasonably close.

In general, the simulated snow covered area compares favorably to the other two. Note in Fig. 11 how much less the unadjusted satellite values are than the others, suggesting that the satellite underestimates snow covered area in this environment. In all 3 years, the snow line method maintained a more rapid decline of snow covered area than the *isnobal* simulation during the main active melt period. This could be attributable to a more accurate depiction in *isnobal* of snow lingering on north facing slopes, whereas the snow line method does not account for this. The higher modelled values of snow covered area during these periods are substantiated at least to some extent by the adjusted satellite values, particularly for 1998 and 1999. Later in the season, the simulated snow

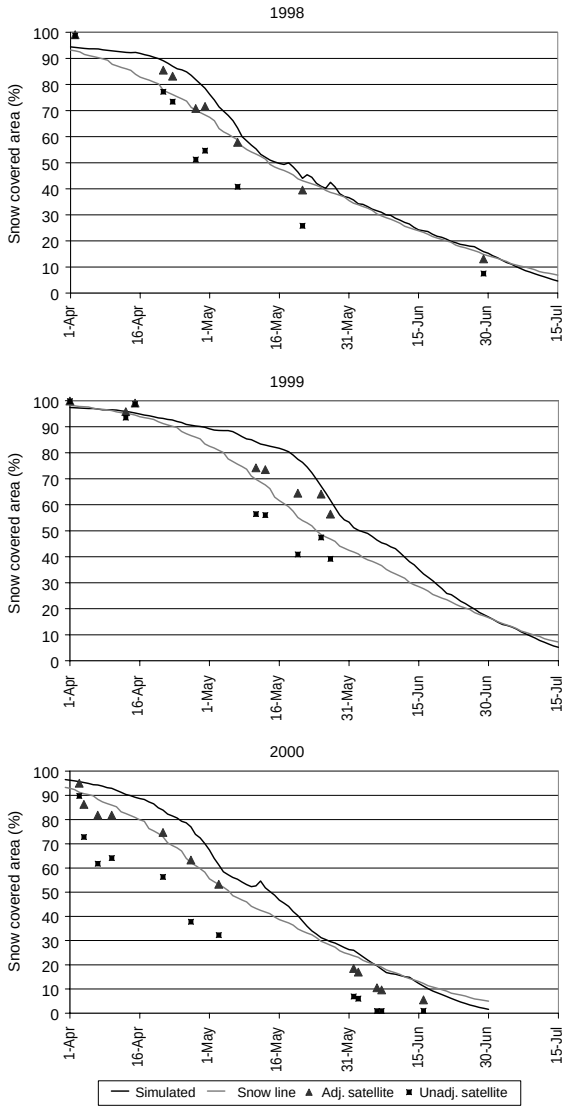

Fig. 11. Snow covered area for 1998–2000 snowmelt seasons as evaluated by different methods. Snow line is from linear regression of melt out date versus elevation for meteorological stations. Adjusted satellite values include forested grid cells where *isnobal* had snow but the satellite image had no snow.

covered area and that from the snow line method coincide closely with one another. In 2000, there was an odd downward jump in the satellite values from 3 April to 4 April, and the values remained low like this for the remainder of the season. The value for 3 April coincided well with the simulated value, but thereafter the satellite values were considerably lower than simulated. It would appear that there could be a systematic error in the satellite values for 2000, since the satellite compared more favorably with the simulations in 1998 and 1999. Because of the resolution and forested area issues with the satellite and because of the simplicity of the snow line method, it is reasonable to expect that the snow covered areas from *isnobal* are often higher. Realizing that none of these values is completely correct, we can only make the judgment that *isnobal* appears to simulate snow covered area reasonably.

Fig. 12 displays the percent of grid cells in agreement between *isnobal* and the satellite as to the designation of the existence snow cover, that is, the percent of grid cells where both indicate snow or both indicate no snow. Percentages with and without the forested cell adjustment for the satellite values are shown; cloud-covered cells are not included in the calculation. The percent agreement starts out high, decreases during the active melt period, then increases again toward the end of the season. This is easy to understand, because at the beginning of the snowmelt period, most grid cells are snow covered, and both methods identify this correctly. Similarly, toward the end of the snowmelt period, most grid cells are snow free, and again, both methods identify this. It is during the active melt period where the ability of each method to discriminate is challenged the most. Nevertheless, the percent agreement was always quite high, with most values including the forest adjustment falling in the 85–95% range. (Without the forest adjustment, the percentages begin and end at about the same values, but during the active melt period, the values are 15–20% lower than those with the adjustment.) The values for 2000 are lower than for 1998 and 1999, but this is due to the low satellite snow covered values noted above. This high degree of agreement in designating snow cover is another positive result indicating the good correspondence between the *isnobal* model and the satellite images.

Fig. 13 shows simulated snow water equivalent fields together with the processed satellite images for selected days during the 1998 snowmelt season. Note that forest adjustments are almost all on the edges of the melted out areas, indicating that the satellite has difficulty identifying as snow covered any areas of low snow water equivalent that are forested. That is,

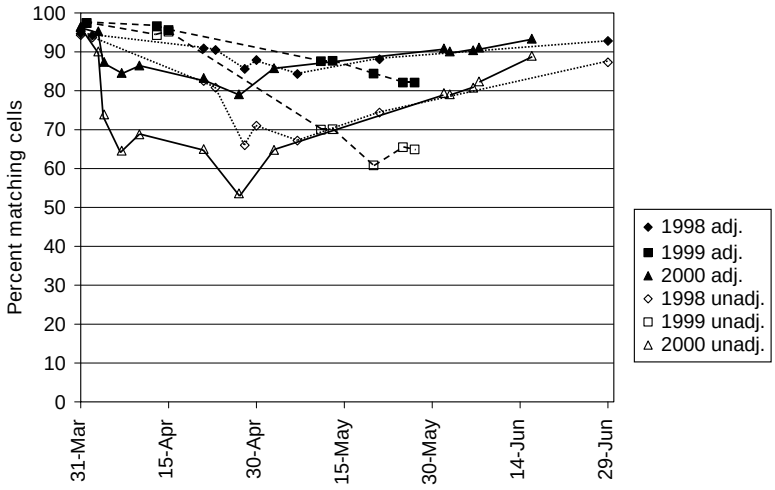

Fig. 12. Percent of grid cells in agreement in designating snow covered or non-snow covered between *isnobal* and satellite. Solid symbols designate values including forest adjustment for satellite, open symbols do not include forest adjustment.

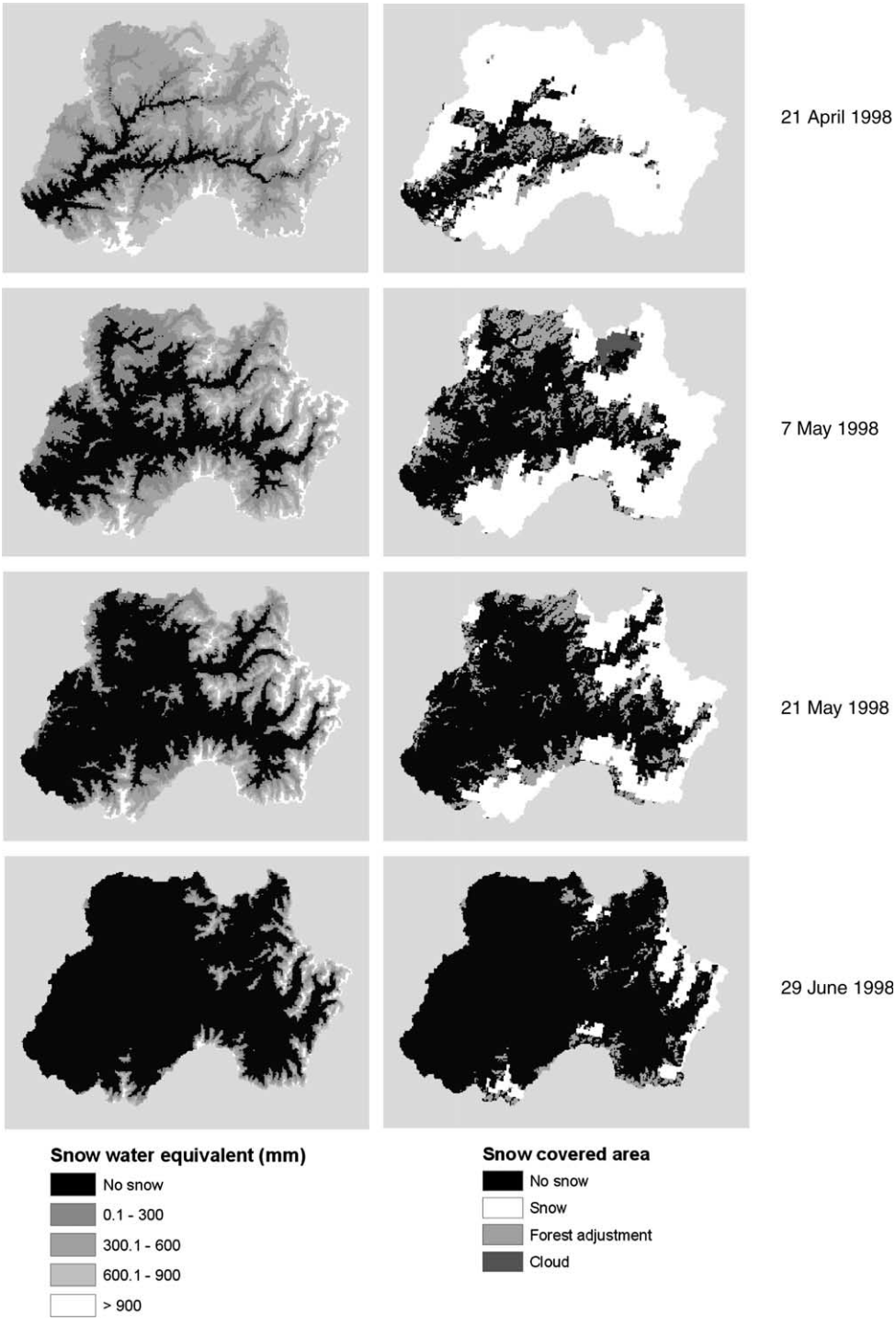

Fig. 13. Snow water equivalent from *isnobal* model and snow covered area from satellite images for 1998. Forest adjustment indicates forested grid cells where *isnobal* had snow but the satellite image had no snow.

the images from the later part of the season show that the satellite recognizes only the major patches of snow. It can also be seen that the dendritic excursions of zero snow up the narrow river valleys shown by *isnobal* do not appear in many of the satellite images; apparently the resolution of the satellite does not allow it to identify these small areas as snow free. Nevertheless, there is quite good visual correspondence between the pairs of images, again providing encouraging confirmation of the *isnobal* simulations.

5.4. Streamflow simulation

The final method of verification represents the next step in the hydrologic modelling of this basin, which is to simulate the water balance and streamflow using the snowmelt model output as moisture input to the land surface and using a water balance model to simulate the water fluxes through the soil system and into the channel system. The water balance and streamflow simulation model used is a grid-based spatially distributed model, developed primarily at the Ruhr Universität Bochum in Germany, described by Garen et al. (2001), Geyer et al. (2001), and Schumann and Garen (1998). Many of the parameters of the model are derived directly from gridded fields of elevation, vegetation, and soil texture. There remain only a few basin-wide parameters that must be evaluated by calibration.

The water balance model was run at a lower spatial and temporal resolution than the snowmelt model because it was judged that the water balance processes did not need to be simulated at such a high resolution and because the water balance model is conceptualized with larger grid cell sizes in mind. The model was, therefore, run with a daily time step and a 1 km^2 grid cell size. This required that the snowmelt model results be aggregated in space and time. The snowmelt depths from *isnobal* were, therefore, accumulated for each day, and fields of the average depth of snowmelt for the set of 16 grid cells within each 1 km^2 water balance model grid cell were computed.

The simulated and observed streamflow for the 1998 snowmelt season is shown in Fig. 14. This represents very preliminary results, since the water balance model is still being tested and modified. Since this was the only year simulated, evaluation of the calibration parameters was done during this period. Only a very basic calibration was done, so this does not represent an optimal streamflow simulation. It was not the purpose at this point to do a full scale optimization and evaluation of the hydrologic model, but rather this exercise was done

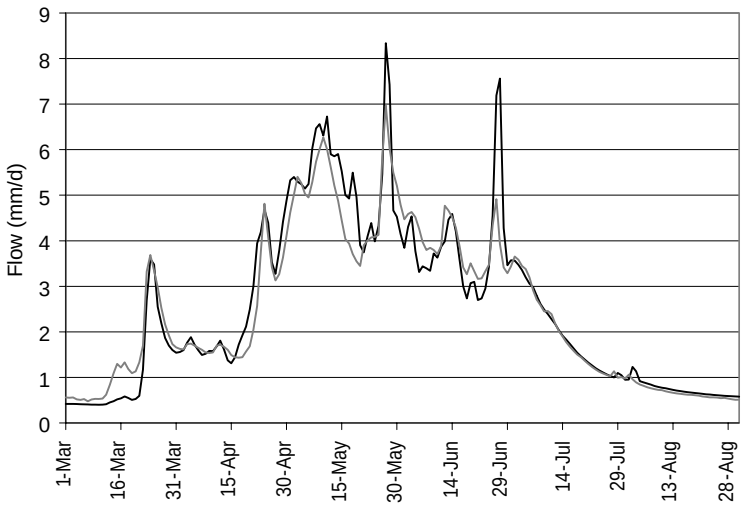

Fig. 14. Simulated (black) and observed (gray) streamflow for 1998 snowmelt season from water balance model using *isnobal* simulated snowmelt as input.

primarily to evaluate the snowmelt model output by seeing if a reasonable streamflow simulation could be achieved.

Given this, the reproduction of the streamflow in Fig. 14 is very satisfactory. Overall, the peaks of the hydrograph occur at the same time as observed, and the recessions follow the observed flows closely. The muted model response to the first hydrograph rise is due to a somewhat misspecified initial soil moisture deficit rather than a lack of snowmelt input. Otherwise, the flow magnitudes are sometimes over- or undersimulated, but this is most likely due to the nonoptimal calibration. The main impression from this simulation is that the snowmelt input obtained from *isnobal* must be quite accurate to allow the rises and falls of the hydrograph to be followed this closely with the water balance model.

6. Conclusion

6.1. Spatial fields of meteorological input data

We have presented the rationale and development steps for procedures used to estimate spatial field time series of the meteorological variables required as input to the spatially distributed snow model *isnobal*. Except for the additional humidity, wind, and radiation sensors, we have used data routinely collected from existing data networks. Due in part to the success of this research, interest and activity is increasing in adding some or all of these sensors to selected SNOTEL stations in various parts of the western US.

Using the procedures presented above, 3 h spatial field time series of precipitation, air temperature, dew point temperature, wind speed, solar radiation, and thermal radiation were computed for the Boise River basin for the years 1998–2000. Though these spatial field time series were developed for *isnobal*, these procedures can also be used for spatially distributed hydrologic modelling in general. For example, the precipitation and air temperature procedures have already been used in several studies (e.g. Geyer et al., 2001). The procedure used to compute net solar radiation fields, while representing the most complex part of the data preparation, should also be quite generally applicable, as should the thermal radiation procedure.

Although the addition of humidity, wind, and radiation sensors to SNOTEL sites was important to the success of this project, some of the difficulties in developing interpolation procedures were associated with the limited elevation range of these sensors. For example, the procedure used to develop the dew point-elevation profiles is dependent on the availability of upper air soundings; in other areas, if these are not available, it would be critical that humidity measurements be taken at the highest elevations possible. Without this, it would be very difficult to distribute humidity spatially over a mountain basin, which is important in determining the precipitation temperature and the latent heat flux. This study shows that the location of the measurement sites is just as important as the variables measured.

Direct verification of these procedures is very difficult, but they can be indirectly verified by evaluating how well the accumulation and ablation of the snowcover and the basin hydrology are simulated, which was very satisfactory. There is still some further checking and fine tuning that could probably be done, however, particularly with the dew point temperature and wind speed procedures.

The collection of data from the additional sensors (humidity, wind, and radiation) installed at three SNOTEL sites was for the most part successful. As data recording systems are modernized, it appears, then, that for selected basins at least, such data could be routinely collected to support more sophisticated modelling efforts. Additional investigation into the performance of the solar and thermal radiometers and their integration into the data recording system would be desirable. For many basins, including the Boise River, it would be worthwhile to consider locating sites higher in the basin to help define better the precipitation, temperature, humidity, and wind trends with elevation.

Using these methods, we are confident that the meteorological inputs for spatially distributed hydrologic models are as good as can be reasonably attained with the given set of stations. The remaining discrepancies between measured and simulated values are most likely due to other sources and can be addressed by parameter calibration, etc. The first prerequisite for a reliable hydrologic simulation, then,

is good input data. It is to be stressed, particularly for spatially distributed models, that significant care and attention be placed on an accurate representation of the spatial variation of the meteorological inputs based on known physical relationships of their behavior in the area to be modelled. We believe that the methods developed in this research accomplish this.

6.2. Snowmelt modelling results

The four methods of verifying the *isnobal* model results, when considered together, indicate that the simulations are reasonable and accurate. Previous applications of *isnobal* and its point version, *snobal*, have shown that, given good input, the model can simulate the snowpack very accurately (Marks et al., 1998, 1999b). This study, then, is a demonstration of the accuracy and reliability of the spatial interpolation methods for preparing the meteorological input fields. These results show that the interpolation methods do a good job of estimating the spatial fields of the relevant meteorological input variables, particularly in light of the constraints of the available data (3 h time step; limited elevation range and representativeness of location characteristics of the data sites; limited solar and thermal radiation data). It, therefore, demonstrates the feasibility of spatially distributed energy budget snowmelt simulation in a relatively large mountainous basin. It also gives an initial indication that the snowmelt model results can be used as input to a spatially distributed water balance model to simulate streamflow and other hydrologically relevant variables (e.g. soil moisture).

6.3. Final remarks

The potential for the routine use of this modelling system to develop informational products to distribute to resource managers is still being contemplated. There are some issues to resolve before it is feasible to use it in an operational environment. For example, it takes many hours to simulate one water year, which is fine in a research mode but is obviously unacceptable for any kind of real time application. This would be less of a constraint for short-term streamflow forecasting but would be a concern for long-range seasonal streamflow forecasting. This situation continually improves, however, with the rapid increase in computer speeds, but then significant investments in new hardware are required to obtain workstations fast enough to reduce the computational time significantly. Another issue is that the data preparation is very time consuming and takes a great deal of manual editing and manipulation, much of which requires human judgment and intervention and may be difficult to automate. With respect to data collection, we have demonstrated that it is feasible to install and collect data from the extra sensors needed for the energy balance approach at remote mountain sites (SNOTEL stations). This does, however, place an additional burden on field personnel for instrument installation and maintenance and for data quality control, in addition to the obvious costs incurred in purchasing the instruments. Even though these extra data are generally considered to be valuable and probably worth the investment, there are political and budget issues that must be resolved before the NRCS or any other government agency can implement a plan for collecting these data on a widespread and routine basis.

Despite these issues, the potential value of this kind of modelling can be envisioned. One clear advantage of such modelling would be the potentially more accurate prediction of streamflow for water management or flood forecasting. This would be especially true during unusual circumstances, such as major runoff events due to rain on snow (as occurred in this area in January 1997), where standard hydrologic models often do not perform well because the energy dynamics are not adequately represented in the model. The use of a spatially distributed model for streamflow prediction would be analogous to the current use of spatially lumped conceptual models, the only difference being that for a spatial model, meteorological forecasts and historical station data (the latter for long-range ensemble forecasts; Day, 1985) will have to be preprocessed into spatial input fields rather than basin areal means. Besides streamflow predictions, the spatially distributed nature of the snowmelt and water balance models lends itself to the generation of new kinds of informational products depicting spatial patterns of snow depth, snow water equivalent, soil moisture, or evapotranspiration, which could be useful in a number of resource management contexts. Such models also have promise for inclusion in

agricultural water quality models to improve their hydrologic basis, and therefore, the prediction of erosion and pollutant loading.

The point of this study has been to demonstrate that it is feasible to use a spatially distributed energy balance snowmelt model in a real-world setting, that is, using data from meteorological stations in an existing network and for a basin whose water, forests, and other resources are actively managed. With continued work, it is envisioned that spatially distributed modelling of this type will form the basis of the next generation of models for water and related resource management.

References

Abramovich, R., Pattee, S., 1999. SNOTEL network-analysis of and future plans for the collection of additional climatic parameters at SNOTEL stations, Proceedings of the Western Snow Conference pp. 137–140.

Anderson, E.A., 1973. National Weather Service River Forecast System-snow accumulation and ablation model, NOAA Technical Memorandum NWS-HYDRO-17, United States Department of Commerce, National Oceanic and Atmospheric Administration, National Weather Service, Washington, DC, USA .

Blöschl, G., Kirnbauer, R., Gutknecht, D., 1991a. Distributed snowmelt simulations in an alpine catchment 1. Model evaluation on the basis of snow cover patterns. Water Resources Research 27 (12), 3171–3179.

Blöschl, G., Gutknecht, D., Kirnbauer, R., 1991b. Distributed snowmelt simulations in an alpine catchment 2. Parameter study and model predictions. Water Resources Research 27 (12), 3181–3188.

Bristow, K.L., Campbell, G.S., Saxton, K.E., 1985. An equation for separating daily solar irradiation into direct and diffuse components. Agricultural and Forest Meteorology 35, 123–131.

Daly, C., Neilson, R.P., Phillips, D.L., 1994. A statistical-topographic model for mapping climatological precipitation over mountainous terrain. Journal of Applied Meteorology 33, 140–158.

Daly, C., Taylor, G.H., Gibson, W.P., Parzybok, T.W., Johnson, G.L., Pasteris, P.A., 2000. High-quality spatial climate data sets for the United States and beyond. Transactions of the American Society of Agricultural Engineers 43 (6), 1957–1962.

Day, G.N., 1985. Extended streamflow forecasting using NWSRFS. Journal of Water Resources Planning and Management 111 (2), 157–170.

Dozier, J., Frew, J., 1990. Rapid calculation of terrain parameters for radiation modeling from digital elevation data. IEEE Transactions on Geoscience and Remote Sensing 28 (5), 963–969.

Dozier, J., Painter, T.H., 2004. Multispectral and hyperspectral remote sensing of alpine snow properties. Annual Review of Earth and Planetary Sciences, in press (available from www.annualreviews.org).

Dubayah, R., Loechel, S., 1997. Modeling topographic solar radiation using GOES data. Journal of Applied Meteorology 36 (2), 141–154.

Dubayah, R.O., Dozier, J., Davis, F.W., 1989. The distribution of clear-sky radiation over varying terrain. Proceedings IGARSS'89, IEEE 89CH2768-0, 885–888.

Dubayah, R., Dozier, J., Davis, F.W., 1990. Topographic distribution of clear-sky radiation over the Konza Prairie, Kansas. Water Resources Research 26 (4), 679–690.

Garen, D.C., 1995. Estimation of spatially distributed values of daily precipitation in mountainous areas. In: Guy, B.T., Barnard, J. (Eds.), Mountain Hydrology: Peaks and Valleys in Research and Applications. Canadian Water Resources Association, Cambridge, Ont., Canada, pp. 237–242.

Garen, D.C., Marks, D., 1996. Spatially distributed snow modelling in mountainous regions: Boise River application. In: Kovar, K., Nachtnebel, H.P. (Eds.), Application of Geographic Information Systems in Hydrology and Water Resources Management, IAHS Publication No. 235. International Association of Hydrological Sciences, Wallingford, Oxfordshire, UK, pp. 421–428.

Garen, D.C., Johnson, G.J., Hanson, C.L., 1994. Mean areal precipitation for daily hydrologic modeling in mountainous regions. Water Resources Bulletin 30, 481–491.

Garen, D.C., Geyer, J., Schumann, A.H., Marks, D., 2001. Spatially-distributed snowmelt, water balance and streamflow modelling for a large mountainous catchment: Boise River, ID, USA. In: Dolman, A.J., Hall, A.J., Kavvas, M.L., Oki, T., Pomeroy, J.W. (Eds.), Soil–Vegetation–Atmosphere Transfer Schemes and Large-Scale Hydrological Models, IAHS Publication No. 270. International Association of Hydrological Sciences, Wallingford, Oxfordshire, UK, pp. 199–207.

Geyer, J., Schumann, A.H., 2001. Large-scale modelling and spatial heterogeneity of landscape characteristics-experiences from the Upper Danube River basin. In: Dolman, A.J., Hall, A.J., Kavvas, M.L., Oki, T., Pomeroy, J.W. (Eds.), Soil–Vegetation–Atmosphere Transfer Schemes and Large-Scale Hydrological Models. IAHS Publication No. 270, International Association of Hydrological Sciences, Wallingford, Oxfordshire, UK, pp. 81–89.

Geyer, J., Garen, D.C., Schumann, A.H., 2001. Improving the representation of water balance and runoff processes in mesoscale hydrologic models for water management modelling. In: Leibundgut, C., Uhlenbrook, S., McDonnell, J. (Eds.), Runoff Generation and Implications for River Basin Modelling, Band 13, Freiburger Schriften zur Hydrologie, Institut für Hydrologie. Universität Freiburg, Germany, pp. 221–228.

Gul, M.S., Muneer, T., Kambezidis, H.D., 1998. Models for obtaining solar radiation from other meteorological data. Solar Energy 64, 99–108.

Hardy, J., Melloh, R., Robinson, P., Jordan, R., 2000. Incorporating effects of forest litter in a snow process model. Hydrological Processes 14, 3227–3237.

Hay, L., Viger, R., McCabe, G., 1998. Precipitation interpolation in mountainous regions using multiple linear regression. In:

Kovar, K., Tappeiner, U., Peters, N., Craig, R. (Eds.), Hydrology, Water Resources and Ecology in Headwaters, IAHS Publication No. 248. International Association of Hydrological Sciences, Wallingford, Oxfordshire, UK, pp. 33–38.

Hudson, G., Wackernagel, H., 1994. Mapping temperature using kriging with external drift: theory and an example from Scotland. International Journal of Climatology 14, 77–91.

Jarvis, C.H., Stuart, N., 2001a. A comparison among strategies for interpolating maximum and minimum daily air temperature. Part I. The selection of 'guiding' topographic and land cover variables. Journal of Applied Meteorology 40, 1060–1074.

Jarvis, C.H., Stuart, N., 2001b. A comparison among strategies for interpolating maximum and minimum daily air temperature. Part II. The interaction between number of guiding variables and the type of interpolation method. Journal of Applied Meteorology 40, 1075–1084.

Kustas, W.P., Rango, A., Uijlenhoet, R., 1994. A simple energy budget algorithm for the snowmelt runoff model. Water Resources Research 30 (5), 1515–1527.

Link, T., Marks, D., 1999a. Distributed simulation of snowcover mass- and energy-balance in the Boreal forest. Hydrological Processes 13, 2439–2452.

Link, T., Marks, D., 1999b. Point simulation of seasonal snowcover dynamics beneath Boreal forest canopies. Journal of Geophysical Research, Atmospheres 104 (D22), 27841–27858.

Marks, D., 1988. Climate, energy exchange, and snowmelt in Emerald Lake watershed, Sierra Nevada. PhD Dissertation, University of California, Santa Barbara, 158pp.

Marks, D., Dozier, J., 1979. A clear-sky longwave radiation model for remote alpine areas. Archiv für Meteorologie, Geophysik und Bioklimatologie, Serie B 27, 159–187.

Marks, D., Kimball, J., Tingey, D., Link, T., 1998. The sensitivity of snowmelt processes to climate conditions and forest cover during rain-on-snow: a case study of the 1996 Pacific Northwest flood. Hydrological Processes 12, 1569–1587.

Marks, D., Domingo, J., Frew, J., 1999a. Software tools for hydroclimatic modeling and analysis, Image Processing Workbench (IPW), ARS-USGS Version 2. ARS Technical Bulletin 99-1, Northwest Watershed Research Center, Agricultural Research Service, Boise, ID, USA. Electronic document available on the Internet at http://www.nwrc.ars.usda.gov/ipw.

Marks, D., Domingo, J., Susong, D., Link, T., Garen, D., 1999b. A spatially distributed energy balance snowmelt model for application in mountain basins. Hydrological Processes 13, 1935.

Marks, D., Link, T., Winstral, A., Garen, D., 2001. Simulating snowmelt processes during rain-on-snow over a semi-arid mountain basin. Annals of Glaciology 32, 195–202.

Marshall, S., Warren, S.G., 1987. Parameterization of snow albedo for climate models. In: Goodison, B., Barry, R., Dozier, J. (Eds.), Large Scale Effects of the Seasonal Snow Cover, IAHS Publication No. 166. International Association of Hydrological Sciences, Wallingford, Oxfordshire, UK, pp. 43–50.

Melloh, R., Hardy, J., Davis, R., Robinson, P., 2001. Spectral albedo/reflectance of littered forest snow during the melt season. Hydrological Processes 15, 3409–3422.

Molotch, N.P., Painter, T.H., Bales, R.C., Dozier, J., 2004. Incorporating remotely sensed snow albedo into spatially distributed snowmelt modeling. Geophysical Research Letters 31, L03501. DOI: 10.1029/2003L019063.

Phillips, D.L., Dolph, J., Marks, D., 1992. A comparison of geostatistical procedures for spatial analysis of precipitation in mountainous terrain. Agricultural and Forest Meteorology 58, 119–141.

Rango, A., Martinec, J., 1995. Revisiting the degree-day method for snowmelt computations. Water Resources Bulletin 31 (4), 657–669.

Rosenthal, W., 1996. Automated snow mapping at subpixel resolution: theoretical bases, practical considerations and programs. CRRLRR-6943-5400, United States Army Cold Regions Research and Engineering Laboratory, Hanover, NH, USA.

Schumann, A.H., Garen, D.C., 1998. Spatially distributed hydrologic modeling for streamflow simulation and forecasting. Proceedings of the First Federal Interagency Hydrologic Modeling Conference, Las Vegas, Nevada, USA, pp. 7.139–7.146.

Susong, D., Marks, D., Garen, D., 1999. Methods for developing time-series climate surfaces to drive topographically distributed energy- and water-balance models. Hydrological Processes 13, 2003–2021.

Tarboton, D.G., Chowdhury, T.G., Jackson, T.H., 1995. A spatially distributed energy balance snowmelt model. In: Tonnessen, K.A., Williams, M.W., Tranter, M. (Eds.), Biogeochemistry of Seasonally Snow-Covered Catchments, IAHS Publication No. 228. International Association of Hydrological Sciences, Wallingford, Oxfordshire, UK, pp. 141–155.

United States Army Corps of Engineers, 1987. Streamflow synthesis and reservoir regulation (SSARR) model user manual. North Pacific Division, Portland, OR, USA.

United States Department of Agriculture—Agricultural Research Service, 1998. Snowmelt runoff model (SRM) user's manual. Electronic document available on the Internet from SRM home page at http://hydrolab.arsusda.gov/cgi-bin/srmhome (actual document address is http://hydrolab.arsusda.gov/pub/srm/srm4.pdf).

University of Oregon, 1999. Pacific Northwest solar radiation data book. Electronic document available on the Internet at http://solardat.uoregon.edu/PacNWSolarRadiationDataBook.html.

Warren, S.G., Wiscombe, W.J., 1980. A model for the spectral albedo of snow. II. Snow containing atmospheric aerosols. Journal of the Atmospheric Sciences 37 (12), 2734–2745.

Wigmosta, M.S., Vail, L.W., Lettenmaier, D.P., 1994. A distributed hydrology–vegetation model for complex terrain. Water Resources Research 30 (6), 1665–1679.

Wiscombe, W.J., Warren, S.G., 1980. A model for the spectral albedo of snow. I. Pure snow. Journal of the Atmospheric Sciences 37 (12), 2712–2733.